12-2023

Quantification of tumor biophysical heterogeneity through mechanical and ultrastructural analysis.

Bradley James Mahaffey
University of Louisville

QUANTIFICATION OF TUMOR BIOPHYSICAL HETEROGENEITY THROUGH MECHANICAL AND ULTRASTRUCTURAL ANALYSIS

By

Bradley James Mahaffey

B.S., Morehead State University, 2019

A Thesis

Submitted to the Faculty of the

J.B. Speed School of Engineering of the University of Louisville

In Partial Fulfillment of the Requirements

for the Degree of

Master of Science in Bioengineering

Department of Bioengineering

University of Louisville

Louisville, Kentucky

December 2023

QUANTIFICATION OF TUMOR BIOPHYSICAL HETEROGENEITY THROUGH MECHANICAL AND ULTRASTRUCTURAL ANALYSIS

By

Bradley Mahaffey

A Thesis Approved on

16 October 2023

By the following Thesis Committee

_____

Joseph Chen
Thesis Chair

_____

Herman Frieboes

_____

Nick Hawkins

ACKNOWLEDGEMENTS

I would like to thank my principal investigator and mentor, Dr. Joseph Chen for his continued support throughout my graduate career. Also, our lab manager and senior-most PhD student, Landon Teer, for his technical advice and inquisitive mindset, helping me round out the rough corners of my thoughts on GBM mechanics. Additionally, my co-first author, Zachary Fowler, for his diligence in SEM characterization and creative collaboration on the text of this manuscript. I would also like to thank the other members of our lab, McKenzie Johnson, Marco Munoz, Neha Anil, Zoe Lung, and Vivien Dang for their persistent dedication to this project and its potential clinical implications.

ABSTRACT

QUANTIFICATION OF TUMOR BIOPHYSICAL HETEROGENEITY THROUGH MECHANICAL AND ULTRASTRUCTURAL ANALYSIS

Bradley J. Mahaffey

16 October 2023

Glioblastoma (GBM) is a highly invasive, aggressive brain cancer that carries a median survival of 15 months. This poor prognosis is due, in part, to its resistance to standard therapeutic intervention. Recent studies have demonstrated that tumor heterogeneity plays a critical role in facilitation therapy resistance by mediating tumor adaptation through microenvironmental cues. Efforts to describe these microenvironmental differences may aid in the development of strategies to combat resistance. GBM can be separated into two distinct regions – a core and a rim, which are thought to drive specific aspects of tumor evolution. The core is proliferative as evidenced by the hypercellular, hypoxic, and necrotic regions while the rim is permissive to cell invasion and spread. These differences in tumor progression are regulated by the diverse biomolecular and biophysical signals in the core and rim, but the biophysical characteristics remain poorly described. Here, we investigate the mechanical and ultrastructural characteristic of the tumor ECM in patient-matched GBM core and rim tissue.

TABLE OF CONTENTS

LIST OF FIGURES

OBJECTIVES

Glioblastoma exhibit extensive heterogeneity in their intra-tumor composition and between patients. Historically, studies have shown that the biology of the tumor microenvironment (TME), and phenotypic manifestations of bulk tumor and mesenchymal cells, display a significant difference in our regions of interest: the core (remodeling) and rim (invasive) regions. This phenomenological study elucidates a connection between GBM regional mechanical signatures and patient demographics/data. These connections between the biomechanical characteristics can pave the way to therapeutic intervention that could improve survival outcomes.

METHODS SUMMARY

Glioblastoma core and rim sections were resected together from 7 patients via craniotomy procedure. Atomic Force Microscopy (AFM) was conducted on each sample to provide stiffness values for mechanical characterization. Scanning Electron Microscopy (SEM) was performed to assess the ultrastructural landscape of each tissue section and supply values for porosity quantification. Immunofluorescence was completed to illustrate and quantify the fluorescent intensity of major structural proteins that make up the brain parenchyma, Tenascin-C and Hyaluronic acid. Simple linear regression was used to uncover prognostic links between these parameters and the independent variables associated with each patient.

RESULTS SUMMARY

AFM reveals spatial heterogeneity and stiffer core tissue. GBM tumors exhibit heterogeneity in mechanical signatures with tumor core exhibiting higher stiffness when compared to tumor rim and to non-neoplastic controls. GBM core exhibits high hyaluronic acid and tenascin-C content ECM analysis of tumor core and rim reveal dramatic expression of HA and Tenascin-C in tumor cores while tumor rim exhibits non-significant increases compared to control tissue. These results suggest that core tissue is actively remodeling its surrounding ECM in a manner conducive to enhanced proliferation. SEM of GBM core displays dense ultrastructure with decreased porosity and pore density. Increased protein density within the ECM of the core and decreased porosity within the core both support the initial AFM findings that found core tissue categorically stiffer than both rim and control. Biophysical signatures of GBM core and rim have prognostic significance. Strong positive correlations were noted with core/rim modulus ratio/overall survival and tenascin-C (rim)/overall survival ($r > .59$). Porosity and pore density at the core both exhibit a modest negative correlation with progression-free survival, with r values of 0.483 and 0.461, respectively. Lastly, HA and TC content at the core also negatively impacted progression free survival, with modest r values of 0.510 and 0.512, respectively.

CONCLUSIONS SUMMARY

Key mechanical differences were elucidated between core and rim tissue in glioblastoma and represent a foundational axis of future therapeutic intervention to improve patient outcomes.

INTRODUCTION

Cancer is a disease that plaques our population with persistence and prevalence, in that 41% of people will develop it, while 20% will succumb to its manifestations [1]. Within this, brain and nervous system cancers account for the cause of death for 5 in every 1,000 people [1]. The nature of cancer is generally well established in that biochemical perturbations disrupt efficient genetic repair and manifest in aggregated DNA damage that manifests in further biochemical dysfunction. However, recently the field of mechanobiology has focused on the haptic considerations of cell fate, behavior, and expression. This dichotomy of interest in the mechanical perspective of tumor progression has spread across the field of cancer research in recent years and is now being actively explored in the context of gliomas. Glioblastoma (GBM), which is the subject of our study, is a highly invasive and aggressive brain cancer, carrying a median survival between 10-14 months and a three-year survival rate of less than 5% [2,3]. GBM is also the most common form of glioma, a larger family of tumors that arise in the central nervous system (CNS), and accounts for approximately 82% of all cases of malignant gliomas [4]. These poor prognoses are due, in part, to GBM's resistance to standard therapeutic intervention, consisting of immediate resection and treatment with the chemotherapeutic drug, temozolomide, due to its ability to cross the blood-brain barrier. As glioblastoma develops, two discrete regions within a given tumor emerge – a proliferative core and a motile, invasive rim. This intratumor heterogeneity is thought to confer the recalcitrant behavior observed throughout disease progression [5,6]. Research efforts have focused on the

biomolecular alterations to the tumor microenvironment (TME) as a driving force of tumor development. Moreover, immunological perspectives have indicated a high concentration of stromal cells, pericytes, and vascular endothelial cells, reflecting the aberrant angiogenesis that is also characteristic of GBM and drives in metabolic requirements forward for progression [7,8,9]. The mechanical tumor microenvironment (TME) is composed of its cellular and extracellular constituents, which are drastically heterogenous in GBM. Non-cancerous immune cells, alongside bulk and specialized tumor cells, create a unique mechanical space the tumor occupies and their functional interplays, coupled with the dense hypoxic environment, drive forward neoplastic replication of bulk tumor cells and increase intracranial pressure (ICP) [7,8,10,11]. Emerging research indicates that biophysical dysregulation of the TME, in addition to these biomolecular alterations, has a significant impact on tumor evolution but remains poorly understood. Ulrich, et al. (2009) [12] showed that the mechanical rigidity of the TME regulates glioma cell morphology, cytoskeletal organization, motility, and proliferation. Further, Grundy et al. (2016) [13] demonstrated the regulation of substrate stiffness on cell speed, a marker for invasive potential. While there are distinctions between GBM and other solid tumors, the remains the altered expression of the hallmark mechanosignaling, master-regulator, YAP/TAZ, that has implications for GBM progression [7]. The brain parenchyma is unique in that its interplay with the surrounding vasculature and white matter tracts facilitate GBM invasion. It has been shown that tumor cells associated with vasculature and these white matter tracts have higher displacement than those without and

provide a neuron-laden highway for increased infiltration [7,14,15]. Concurrently with GBM progression, ECM components are upregulated, which have been shown to contribute to ECM stiffening [16]. Of this array of ECM proteins, hyaluronic acid and tenascin-C represent the crux of our immunofluorescent study of the aberrantly overexpressed native proteins. Expected values for these increased stiffness GBM tissues can range up to 45kPa, heavily activating the mechanotransductive cascade of biomolecules within GBM cells [7,17,18,19]. The mechanical perspective on GBM recurrence and aggressiveness has been demonstrated to be rooted in ECM remodeling to a stiffer phenotype, even present in the less aggressive IDH1- mutant gliomas, leading to a linear force driven positive feedback loop that remodels tenascin-C content through expression changes caused by reduced miR-203 suppression of HiF1alpha [20]. Of note for consideration of lower stiffness values that represent regions of distinct mechanical heterogeneity, there exists significant ECM remodeling through upregulated matrix metalloproteinase (MMP) activity, which will degrade ECM and invert the typical hypercellular, hypoxic stiffening narrative for GBM [21]. On the other hand of heterogeneity, the stiffening ECM activates mechanosensors, like focal adhesion kinas (FAK) and leads to its overexpression [22]. Associated with FAK and mechanosensing, GBM also experiences dysregulation of integrins expressed on its cellular membrane and thus misinterprets the ECM stress into its actin cytoskeleton and down the transductive chain to influence its nuclear expression of ECM deposition, structural proteins, and cytokines, along with its attachment to the ECM for

migratory purposes [23,24,25]. The presence of F-actin in the ECM is another key driver of GBM progression in that the dysregulated integrins erroneously transduce altered interpretations of the F-actin network in the ECM, which there signal downstream cascades to deposit more ECM which stiffens its immediate vicinity and favors GBM's invasion and migratory phenotype [26]. One of the critical mechanosensing adhesion receptors, CD44, binds to hyaluronic acid and allows for transduction and subsequent manipulation and movement through the local parenchyma [27,28]. This interaction between CD44 and HA has been shown to drive the progression of GBM through proliferation and invasion by activation of Rho GTPases, remodeling of invadopodia, and activation of PI3K/Akt and MAP/ERK [29]. The mechanical cascade of ECM remodeling does not even spare ion channels from dysregulation, in that Piezo1, which has been implicated in disease states of other cancers and atherogenesis in vascular malformations and bifurcations, has shown overexpression in GBM [30]. Lastly, the Hippo signaling pathway, that is the spectrum of expression in mechanosensing regulatory proteins and controls the balance between proliferation and apoptosis, finds itself in disarray in GBM [31]. This dysregulation is characteristic of the master regulators being phosphorylated, due to increased mechanical sensing, which maintains them in an inactive cystolic state. We expect this to be the case in the study of our patient matched GBM tissue and, despite literature supporting the role of biophysical changes in tumor aggressiveness, there has been no quantification of these alterations in human

patients. Here, we investigate the mechanical and ultrastructural characteristics of the TME in patient matched GBM core and rim tissue.

METHODS

Patient sample tissue and gene status collection

In cooperation with Baxter et al. 2023 [32], all specimens were collected following approved Internal Review Board protocols at University of Louisville Hospital (IRB 20.0219) from patients with known or suspected brain tumors. As brain cancer affects both women and men, samples from both were collected. Samples were collected by the clinical team, blinded to the research analysis. Patient information was de-identified by the clinical team before evaluation by the research team. IDH-R132H mutation was detected by immunohistochemistry and MGMT promoter methylation by next generation sequencing (Neogenomics Inc., Fort Meyers, FL). Informed consent was obtained to participate in this study.

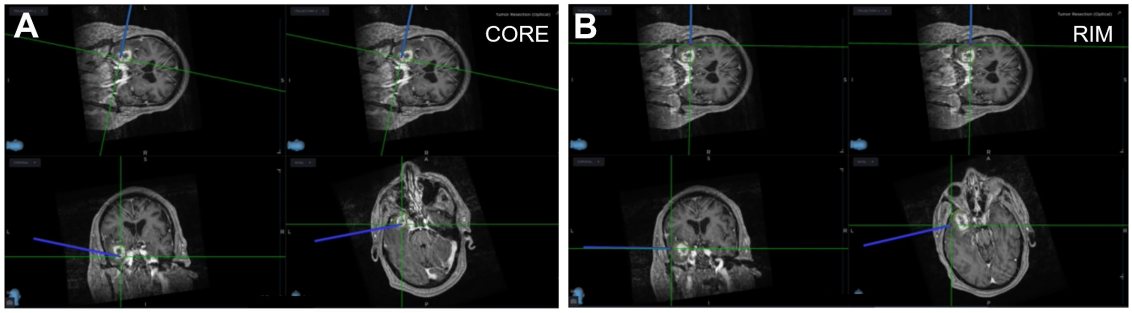

Figure 1. Intraoperative 3D navigation view of GBM core and rim. Tumor biopsies were extracted within the tumor, designated as tumor core (A), and within the invasive margin of the tumor, designated as tumor rim (B).

Mechanical Characterization via AFM

Sample preparation was performed via cryotome sectioning of patient matched brain tissue samples in to 50 μm sections that were deposited onto charged glass slides. Charging facilitates the adhesion of the tissue to the glass and

maintains its structural integrity in the following phases of characterization. Each section will be prepared for AFM by use of a hydrophobic pen to encircle the tissue on the glass slide. PBS will then be deposited onto the slide in the circle. The PBS will dissolve the OCT biological adhesive so as to not confound stiffness measurements. Calibration of the AFM and cantilever must be done in the liquid phase to fit the spectra of the cantilever's thermal oscillations in liquid. The design of the experiment will include use of Asylum AFM and Bruker MLCT-BIO cantilevers to deform the surface of the samples and record a series of force maps composed of individual force curves. Each will have their own stiffness values, determined by the force offset and indentation starting points, along with the curvature recorded for extension into the sample. A Poisson ratio of 0.5 is to be used for brain tissue. Given the Hertzian model for elastic modulus, fitting the shape of the deforming effector, the cantilever can be approximated to a cone with a half angle of 36°. The stiffness value for the cantilever's silicon nitride material composition is 290 GPa. Any reciprocal deformation caused by the brain onto the cantilever material is negligible.

For data acquisition purposes of tissue samples: a scan size of 20umx20um (max) is used with 16x16 pixel resolution yields 256 data points per force map. 5 force maps are acquired per section and 3 sets of 256 are processed, giving an average stiffness and distribution for each patient. Adjacent sections have been reserved for further processing via decellularization and SEM to compare any morphologically notable regions.

Tissue Decellularization and Preparation

Prior to collection, tissue was coated in OCT and stored at -80℃. The tissue was thawed and uncovered at room temperature for 60 minutes. Hydrophobic pen was used to outline the tissue on the microscope slide, allowing for improved visualization and to contain the reagents to be later applied. Decellularization protocol was performed as follows: (1) Wash in tissue in PBS for 20 minutes at room temperature. Remove PBS and let tissue dry at room temperature for 10 minutes. (2) Wash tissue in deionized water for 5 minutes at room temperature. Remove deionized water and let tissue dry at room temperature for 10 minutes. (3) Wash tissue in 0.1% sodium deoxycholate (SD) for 15 minutes at 37℃. Remove SD and allow tissue to dry at room temperature for 10 minutes. (4) Repeat (3). (5) Wash tissue in PBS for 5 minutes at room temperature. (6) Repeat (5) two additional times. (7) Wash tissue in DNAse I solution for 35 minutes at 37℃. Remove DNAse I solution and let samples dry at room temperature for 10 minutes. Note: DNAse I solution comprised of 0.260 mL v/v DNAse I in buffer. (8) Wash tissue in PBS for 5 minutes at room temperature. (9) Repeat (8) two additional times.

Immunofluorescent Staining and Quantification

Immediately after completion of the final PBS wash described previously, samples were fixed in a 1:10 formalin in PBS solution for 15 minutes at room temperature. Two consecutive PBS washes for 5 minutes each, which a 10-minute drying period in between, followed fixation. Immunostaining protocol was performed as follows: (1) Flood samples with Intercept Blocking Buffer for one

hours. Remove buffer from the samples. (2) Apply primary antibodies for hyaluronic acid (HA) and tenascin-C (TC) at 1:200 dilution and let sit, covered, at room temperature for 4 hours or overnight at -20℃. (4) Remove primary antibodies and perform three consecutive PBS washes with a 10-minute drying period in between each at room temperature. Keep samples protected from light when not actively washing or removing reagents. (5) Apply secondary antibodies in a 1:200 dilution for one hour, covered, at room temperature. (6) Remove the secondary antibodies and perform two consecutive PBS washes with a 10-minute drying period in between. (7) Apply DAPI mounting media to the microscope slide adjacent to the tissue and overlay a glass coverslip such that the DAPI mounting media is spread evenly across the tissue. Let sit for minimum of 4 hours, covered, at room temperature to allow the media to cure.

Fluorescence area and intensity was calculated using protocol established by the University of Maryland, Baltimore County (UMBC) College of Natural and Mathematical Sciences (cite). Fluorescence intensity is directly proportional to the concentration of the protein-of-interest within the ECM. Analysis was performed on ImageJ (FIJI) as follows:

Fluorescent Area: (1) Used the Color Threshold command to image threshold was adjusted such that the hue slider matched the color of the fluorescent area. (2) Used the Analyze Particles command to display the areas of fluorescence that were at or above threshold. (3). Summed all areas of fluorescence detected to calculated Total Fluorescent Area.

Fluorescent Intensity: (1) Outlined the desired area of tissue using the shape or freehand commands. (2) Used the Set Measurements command to include area, integrated density, and mean grey value in the results. (3) Copied the resulting data points into a spreadsheet. (4) Repeated (2) and (3) but instead, outline an area without fluorescence. This represents the background. (5) Calculated the mean fluorescence for each of the areas outlined. Excluded background from this calculation. (6) Corrected Total Fluorescence (CTF) was subsequently calculated as follows:

$$CTF = Integrated\ Density - \frac{Total\ Fluorescent\ Area}{Background\ Fluorescence} \quad (1)$$

SEM Preparation

Sample preparation for SEM imaging was performed as follows: (1) Soak tissue in 2.5% glutaraldehyde solution in 0.1M sodium cacodylate (pH 7.4) and let sit at room temperature for 20 minutes. Store at -20℃ for 12-24 hours following. (2) Rinse samples in 0.1M PBS three times for five minutes each at room temperature. (3) Samples fixed in 1% osmium tetroxide for 30 minutes at room temperature. (4) Rinse samples with deionized water three times for 10 minutes each. (5) Dehydrate samples by sequentially flooding with 50%, 70%, and 95% EtOH for 10 minutes each.

Prior to imaging, Cressington Vacuum Coating System for Au and Au/Pd was used to sputter coat decellularized tissue for 30 seconds or to approximately 7nm thickness. Images of processed samples were obtained via Apreo C LoVac

FESEM (ThermoScientific) at a working distance between 11-15mm, high voltage (5.00kV), using the Everhart-Thornley Detector (ETD), and magnification ranging from 200X to 2000X based on the size of the sample.

Ultrastructural Characterization

Image processing was performed using ImageJ (FIJI) software. The following protocol was performed on images of both the core and the rim of each patient: (1) Image file is loaded into ImageJ. (2) Using the scale bar provided on the SEM image file, scale was set in ImageJ accordingly. (3) Image was duplicated to remove the information banner. (4) Image type changed to 8-bit. (5) Brightness & Contrast adjusted to maximize the contrast between tissue space and porous space. (6) Threshold adjusted and set to black & white (B&W). (7) Fill Holes command use to increase the continuity of the porous space. (8) Total area of the image was calculated and recorded. (9) Within the Analyze Particles command, bounds on particle size were set to 1.0um2-infinity. Circularity bounds set to 0.1-0.99. (10) Display Results, Include Holes, and Composite ROIs results were selected. This data was used to calculate porosity, average pore size (um2), and pore density (pores/μm^2). The total number of particles detected within the given bounds reflects the number of pores present in the tissue. See equations below.

$$Porosity = \frac{Total\ Porous\ Area}{Total\ Image\ Area} \quad (2)$$

$$Average\ Pore\ Size = \frac{Total\ Porous\ Area}{Total\ Number\ of\ Pores} \quad (3)$$

$$Pore\ Density = \frac{Total\ Number\ of\ Pores}{Total\ Image\ Area} \quad (4)$$

RESULTS

AFM reveals spatial heterogeneity and stiffer core tissue. GBM tumors exhibit heterogeneity in mechanical signatures with tumor core exhibiting higher stiffness when compared to tumor rim and to non-neoplastic controls (Figure 2A). However, the relative differences between tumor core and rim are patient specific (Figure 2B).

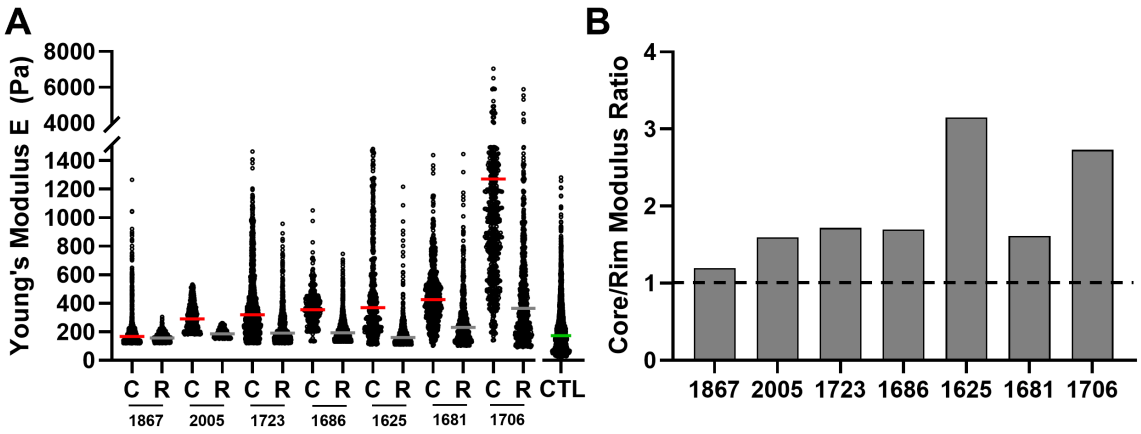

Figure 2. AFM reveals spatial heterogeneity and stiffer core tissue. GBM tumor exhibit heterogeneity in mechanical signatures with tumor core exhibiting higher stiffness when compared to tumor rim and to non-neoplastic controls (A). However, the relative differences between tumor core and rim is patient specific (B).

Using AFM, we found that core tissue is uniformly stiffer than both patient-matched rim tissue and non-neoplastic control tissue. The magnitude of this stiffness increase is patient-specific, as displayed by the core/rim modulus ratios in Figure 2A, which range from 1.19-3.15. These mechanical differences are likely due to a combination of biomolecular and biophysical cues from the TME.

GBM core exhibits high hyaluronic acid and tenascin-C content ECM analysis of tumor core and rim reveal dramatic expression of HA and Tenascin-C in tumor

cores while tumor rim exhibits non-significant increases compared to control tissue (Figure 3A-C).

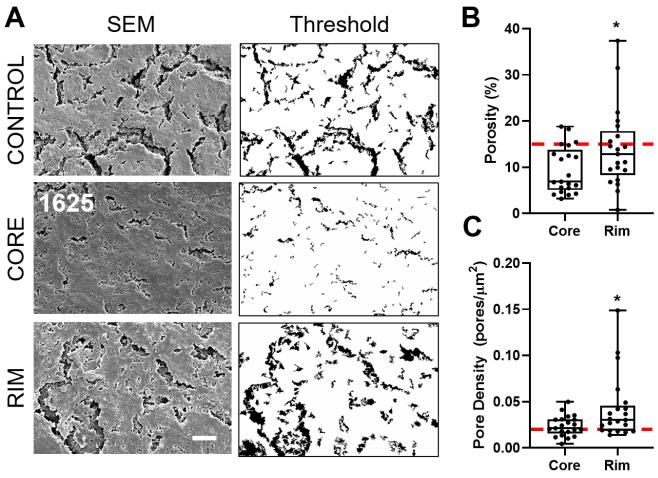

Figure 3. GBM core displays dense ultrastructure with decreased porosity and pore density SEM analysis reveals decreased porosity within tumor cores when compared to tumor rim and control samples (A,B). Pore density, the number of pores per area, was also lower in tumor core (C); * - p< 0.05, scalebar = 10 μm

Mohiuddin and Wakimoto (2021) [33] describe the dysregulation of ECM proteins, including hyaluronic acid (HA) and tenascin-C (TC), in GBM associated with increased overall density and stiffness. Our exploration of ECM composition via IF staining revealed that core tissue exhibits elevated levels of both HA and TC compared to rim and control tissues. Elevated expression of HA and TC was also observed in the rim with respect to control, but this difference was not significant. These results suggest that core tissue is actively remodeling its surrounding ECM in a manner conducive to enhanced proliferation.

GBM core displays dense ultrastructure with decreased porosity and pore density SEM analysis reveals decreased porosity within tumor cores when compared to tumor rim and control samples (Figure 4A, 4B). Pore density, the number of pores per area, was also lower in tumor core (Figure 4C).

The mechanical and compositional changes seen previously demanded exploration of potential ultrastructural consequences. Using standard porosity quantifications methods, we found tumor core tissue was less porous than rim and non-neoplastic control and had decreased pore density, defined as pores/um2. Increased protein density within the ECM of the core (Figure 3) and decreased porosity within the core (Figure 4) both support the initial AFM findings that found core tissue categorically stiffer than both rim and control.

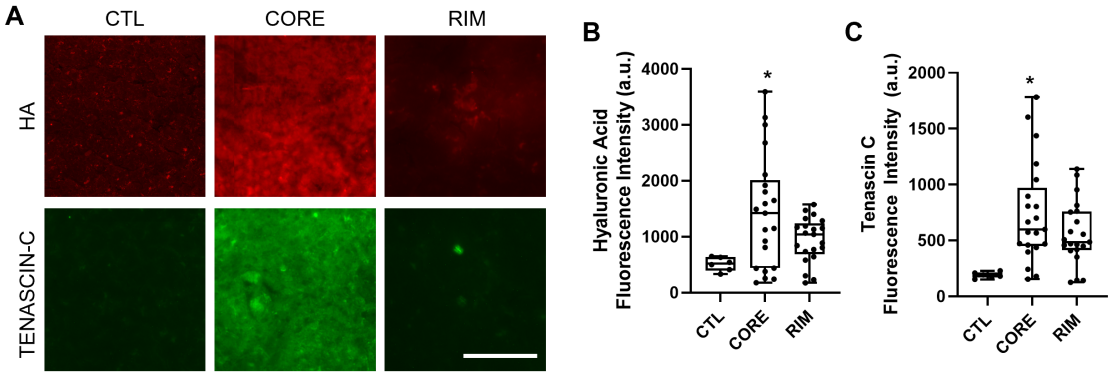

Figure 4. GBM core exhibits high hyaluronic acid and tenascin-C content ECM analysis of tumor core and rim reveal dramatic expression of HA and Tenascin-C in tumor cores while tumor rim exhibits non-significant increases compared to control tissue (A-C). Scalebar = 100 μm

Biophysical signatures of GBM core and rim have prognostic significance Strong positive correlations were noted with core/rim modulus ratio/overall survival and tenascin-C (rim)/overall survival (r >.59) (Figure 5A, 5B), while moderate negative correlations were observed with porosity (Core)/progression free survival, pore density (Core)/progression free survival, HA (Core)/progression free survival, Tenascin-C (Core)/progression free survival.

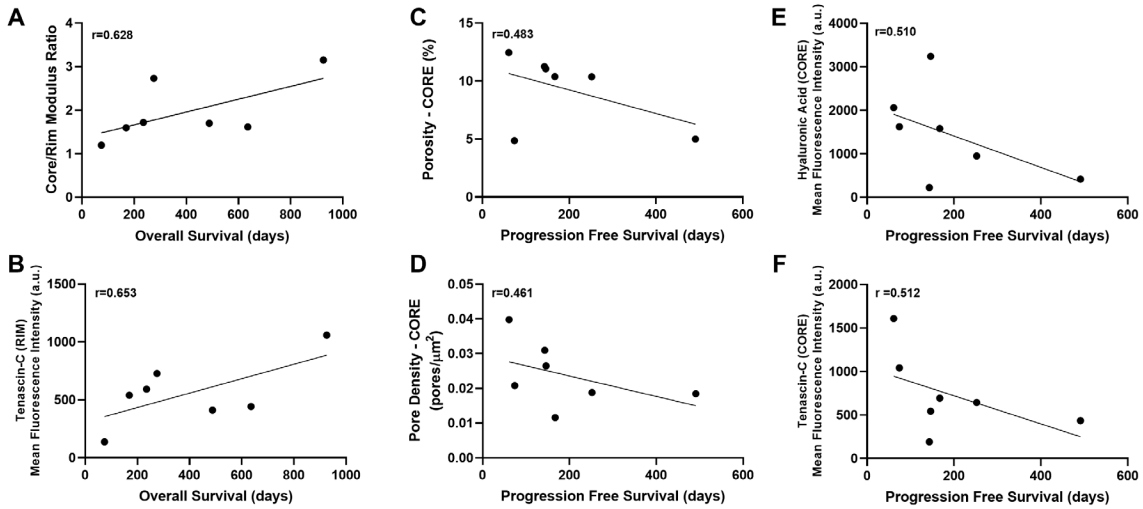

Figure 5. Biophysical signatures of GBM core and rim have prognostic significance Strong positive correlations were noted with core/rim modulus ratio/overall survival and tenascin-C (rim)/overall survival (r >.59) (A,B), while moderate negative correlations were observed with porosity (Core)/progression free survival, pore density (Core)/progression free survival, HA (Core)/progression free survival, Tenascin-C (Core)/progression free survival.

Using overall and progression-free survival, we then examined the prognostic influence of these biophysical alterations. A Spearman correlation was used in place of its counterpart, the Pearson correlation, due to the possible non-linear relationship in these variables. The spearman correlation functioned to provide a composite score for the ability of our data to fit a monotonically increasing or decreasing function. Processing of the data did show that a linear function provided the bet fit and was thus plotted (Figure 5). The core/rim stiffness ratio has a strong, positive correlation with overall survival with a spearman correlation coefficient of 0.628 (Figure 5A). The concentration of TC at the rim is also strongly correlated with overall survival (r = 0.653, Figure 5B). Porosity and pore density at the core both exhibit a modest negative correlation with progression-free survival, with r values of 0.483 and 0.461, respectively (Figures 5C and 5D). Lastly, HA and TC content at the core also negatively impacted progression free

survival, with modest r values of 0.510 and 0.512, respectively (Figures 5E and 5F).

DISCUSSION

The heterogenous nature of the TME underlies many of the challenges in treating GBM and there is an important need to better understand the components of the TME that promote disease evolution. Changes in the biophysical compartment of the TME are still poorly understood, and clarifying these characteristics will generate new insights and avenues of approach for overcoming TME-dependent drivers of GBM progression. These insights can then be leveraged in the conception of TME-oriented therapies to combat therapeutic resistance and improve prognosis. Here we have shown that the overarching trend of stiffer core and softer rim present in our data support existing literature. Aubry, et al. (2015) [34] describe core tissue as a “necrotic zone,” which is supported by our evidence of enhanced remodeling in the core. We also supply new information on the tumor rim, as we find that the invasive margins (the interface between healthy tissue and tumor rim) experiences less remodeling, have ECM protein concentrations similar to control, and retain mechanical properties similar to surrounding parenchyma. The ECM changes are also consistent with current research: Miroshnikova, et al., (2016) [35] demonstrated increased mechanosignaling in GBM as a result of Tenascin-C’s ability to cross-link HA, increasing the overall stiffness of the TME. HA and TC content at the rim is significantly lower than the core, which suggests that the ECM effects dominate in the core, phenotypically altering the invading cells, and activating them with enhanced ECM signals prior to reaching the invasive margin. Optically, our SEM study has elucidated that the core is denser that the rim. This is consistent with

previous literature confirming elevated density in the core region. Rim is identified as more porous which supporting literature implicates as favorable for invasion of necroticly remodeled core cells. Our findings yield new insights that elevated core ECM proteins (HA and Ten-C) lead to poorer prognosis in that increased concentration may facilitate increased mechanotransduction that is associated with pro-malignant phenotypes and downstream signaling pathways. By this notion it would be expected that a stiff core would also correlate with poor prognosis. Paradoxically, it appears a “Goldilocks zone” of sorts exists, such that prognosis is negatively affect up to a point, at which core stiffness begins to confer limitations on GBM cell migration ability, intratumorally, not allowing easy passage to even the rim region. This is consistent with previous literature that has shown 3D invasion is reduced with increased density [36]. Extending this sentiment, we have shown that increased Ten-C content at the rim confers improved survival, being that Ten-C is associated with cross-linking of ECM proteins, this suggests that GBM cells trying to invade may experience a more challenging, denser landscape to navigate than tumors that have more permissive rim content. Porosity trends did not show this trend but may be illuminated by greater sample size as our cohort study progresses. Increased core/rim stiffness modulus ratio was shown to lead to improved survival in our study. This may indicate a dramatic mechanical change at the interface of core and rim can limit invasion. Cell durotaxis, which is implicated for this transition, limits cell ability to migrate from stiff to soft matrix, and the intratumoral heterogeneity that is apparent in our patient samples represents an explanation

for the improved survival that accompanies it. This suggests that GBM cell's mechanical environments may direct invasion path, not exclusively chemokines. This is to our knowledge the first report on the biophysical characteristics of the GBM TME. These data show the broad mechanical, ECM, and ultrastructural changes in GBM, but also reveal dramatic differences between patients. Details in sex, age, race should be assessed in larger cohorts to identify trends/effects of these variables. It is likely that with a larger set of patient data, the Spearman test could yield nonlinear relationships between our parameters, namely the Core/Rim modulus ratio. Recognition of limits in these biophysical effects indicate the nuance of biophysical cues; dense matrix is pro-pathological but too dense improves survival. Core/rim ratio is generally a hallmark of GBM, but too big of a ratio can slow disease progression. Additional investigations with larger cohorts can generate deeper insights and identify important biophysical features that can be used in diagnostic and therapeutic spaces.

REFERENCES

1. *Lifetime Risk of Developing or Dying From Cancer*. (n.d.). Retrieved August 3, 2023, from https://www.cancer.org/cancer/risk-prevention/understanding-cancer-risk/lifetime-probability-of-developing-or-dying-from-cancer.html
2. Dubrow, R., & Darefsky, A. S. (2011). Demographic variation in incidence of adult glioma by subtype, United States, 1992-2007. *BMC Cancer*, *11*(1), 325. https://doi.org/10.1186/1471-2407-11-325
3. Krex, D., Klink, B., Hartmann, C., von Deimling, A., Pietsch, T., Simon, M., Sabel, M., Steinbach, J. P., Heese, O., Reifenberger, G., Weller, M., Schackert, G., & German Glioma Network. (2007). Long-term survival with glioblastoma multiforme. *Brain: A Journal of Neurology*, *130*(Pt 10), 2596–2606. https://doi.org/10.1093/brain/awm204
4. Dolecek, T. A., Propp, J. M., Stroup, N. E., & Kruchko, C. (2012). CBTRUS Statistical Report: Primary Brain and Central Nervous System Tumors Diagnosed in the United States in 2005–2009. *Neuro-Oncology*, *14*(Suppl 5), v1–v49. https://doi.org/10.1093/neuonc/nos218
5. Hoelzinger, D. B., Mariani, L., Weis, J., Woyke, T., Berens, T. J., McDonough, W. S., Sloan, A., Coons, S. W., & Berens, M. E. (2005). Gene expression profile of glioblastoma multiforme invasive phenotype points to new therapeutic targets. *Neoplasia (New York, N.Y.)*, *7*(1), 7–16. https://doi.org/10.1593/neo.04535
6. Alfardus, H., de Los Angeles Estevez-Cebrero, M., Rowlinson, J., Aboalmaaly,

7. A., Lourdusamy, A., Abdelrazig, S., Ortori, C., Grundy, R., Kim, D.-H., McIntyre, A., & Smith, S. (2021). Intratumour heterogeneity in microRNAs expression regulates glioblastoma metabolism. *Scientific Reports*, *11*(1), 15908. https://doi.org/10.1038/s41598-021-95289-9
8. Pontes, B., & Mendes, F. A. (2023). Mechanical Properties of Glioblastoma: Perspectives for YAP/TAZ Signaling Pathway and Beyond. *Diseases*, *11*(2), Article 2. https://doi.org/10.3390/diseases11020086
9. Alexander, B. M., & Cloughesy, T. F. (2017). Adult Glioblastoma. *Journal of Clinical Oncology: Official Journal of the American Society of Clinical Oncology*, *35*(21), 2402–2409. https://doi.org/10.1200/JCO.2017.73.0119
10. Cruz, J. V. R., Batista, C., Afonso, B. de H., Alexandre-Moreira, M. S., Dubois, L. G., Pontes, B., Moura Neto, V., & Mendes, F. de A. (2022a). Obstacles to Glioblastoma Treatment Two Decades after Temozolomide. *Cancers*, *14*(13), 3203. https://doi.org/10.3390/cancers14133203
11. Reetz, K., Abbas, Z., Costa, A. S., Gras, V., Tiffin-Richards, F., Mirzazade, S., Holschbach, B., Frank, R. D., Vassiliadou, A., Krüger, T., Eitner, F., Gross, T., Schulz, J. B., Floege, J., & Shah, N. J. (2015). Increased Cerebral Water Content in Hemodialysis Patients. *PLOS ONE*, *10*(3), e0122188. https://doi.org/10.1371/journal.pone.0122188
12. Ciasca, G., Sassun, T. E., Minelli, E., Antonelli, M., Papi, M., Santoro, A., Giangaspero, F., Delfini, R., & Spirito, M. D. (2016). Nano-mechanical signature

of brain tumours. *Nanoscale*, *8*(47), 19629–19643. https://doi.org/10.1039/C6NR06840E

13. Ulrich, T. A., de Juan Pardo, E. M., & Kumar, S. (2009). The mechanical rigidity of the extracellular matrix regulates the structure, motility, and proliferation of glioma cells. *Cancer Research*, *69*(10), 4167–4174. https://doi.org/10.1158/0008-5472.CAN-08-4859
14. Grundy, T. J., De Leon, E., Griffin, K. R., Stringer, B. W., Day, B. W., Fabry, B., Cooper-White, J., & O'Neill, G. M. (2016). Differential response of patient-derived primary glioblastoma cells to environmental stiffness. *Scientific Reports*, *6*(1), Article 1. https://doi.org/10.1038/srep23353
15. Farin, A., Suzuki, S. O., Weiker, M., Goldman, J. E., Bruce, J. N., & Canoll, P. (2006). Transplanted glioma cells migrate and proliferate on host brain vasculature: A dynamic analysis. *Glia*, *53*(8), 799–808. https://doi.org/10.1002/glia.20334
16. Winkler, F., Kienast, Y., Fuhrmann, M., Von Baumgarten, L., Burgold, S., Mitteregger, G., Kretzschmar, H., & Herms, J. (2009). Imaging glioma cell invasion in vivo reveals mechanisms of dissemination and peritumoral angiogenesis. *Glia*, *57*(12), 1306–1315. https://doi.org/10.1002/glia.20850
17. Quail, D. F., & Joyce, J. A. (2017). The Microenvironmental Landscape of Brain Tumors. *Cancer Cell*, *31*(3), 326–341. https://doi.org/10.1016/j.ccell.2017.02.009
18. Barnes, J. M., Przybyla, L., & Weaver, V. M. (2017). Tissue mechanics regulate

brain development, homeostasis and disease. *Journal of Cell Science*, *130*(1), 71–82. https://doi.org/10.1242/jcs.191742

19. Li, X., & Wang, J. (2020a). Mechanical tumor microenvironment and transduction: Cytoskeleton mediates cancer cell invasion and metastasis. *International Journal of Biological Sciences*, *16*(12), 2014–2028. https://doi.org/10.7150/ijbs.44943
20. Stewart, D. C., Rubiano, A., Dyson, K., & Simmons, C. S. (2017). Mechanical characterization of human brain tumors from patients and comparison to potential surgical phantoms. *PloS One*, *12*(6), e0177561. https://doi.org/10.1371/journal.pone.0177561
21. Miroshnikova, Y. A., Mouw, J. K., Barnes, J. M., Pickup, M. W., Lakins, J. N., Kim, Y., Lobo, K., Persson, A. I., Reis, G. F., McKnight, T. R., Holland, E. C., Phillips, J. J., & Weaver, V. M. (2016b). Tissue mechanics promote IDH1-dependent HIF1α-tenascin C feedback to regulate glioblastoma aggression. *Nature Cell Biology*, *18*(12), 1336–1345. https://doi.org/10.1038/ncb3429
22. DE Oliveira Rosario, L. V., DA Rosa, B. G., Goncalves, T. L., Matias, D. I. L., Freitas, C., & Ferrer, V. P. (2020). Glioblastoma Factors Increase the Migration of Human Brain Endothelial Cells In Vitro by Increasing MMP-9/CXCR4 Levels. *Anticancer Research*, *40*(5), 2725–2737. https://doi.org/10.21873/anticanres.14244
23. Rutka, J. T., Muller, M., Hubbard, S. L., Forsdike, J., Dirks, P. B., Jung, S., Tsugu,

A., Ivanchuk, S., Costello, P., Mondal, S., Ackerley, C., & Becker, L. E. (1999). Astrocytoma Adhesion to Extracellular Matrix: Functional Significance of Integrin and Focal Adhesion Kinase Expression. *Journal of Neuropathology & Experimental Neurology*, *58*(2), 198–209. https://doi.org/10.1097/00005072-199902000-00009

24. Belot, N., Rorive, S., Doyen, I., Lefranc, F., Bruyneel, E., Dedecker, R., Micik, S., Brotchi, J., Decaestecker, C., Salmon, I., Kiss, R., & Camby, I. (2001). Molecular characterization of cell substratum attachments in human glial tumors relates to prognostic features. *Glia*, *36*(3), 375–390. https://doi.org/10.1002/glia.1124
25. Friedlander, D. R., Zagzag, D., Shiff, B., Cohen, H., Allen, J. C., Kelly, P. J., & Grumet, M. (1996). Migration of Brain Tumor Cells on Extracellular Matrix Proteins in Vitro Correlates with Tumor Type and Grade and Involves αv and β1 Integrins1. *Cancer Research*, *56*(8), 1939–1947.
26. Paulus, W., Baur, I., Schuppan, D., & Roggendorf, W. (1993). Characterization of integrin receptors in normal and neoplastic human brain. *The American Journal of Pathology*, *143*(1), 154–163.
27. Koh, I., Cha, J., Park, J., Choi, J., Kang, S.-G., & Kim, P. (2018). The mode and dynamics of glioblastoma cell invasion into a decellularized tissue-derived extracellular matrix-based three-dimensional tumor model. *Scientific Reports*, *8*(1), Article 1. https://doi.org/10.1038/s41598-018-22681-3
28. Pietras, A., Katz, A. M., Ekström, E. J., Wee, B., Halliday, J. J., Pitter, K. L.,

Werbeck, J. L., Amankulor, N. M., Huse, J. T., & Holland, E. C. (2014). Osteopontin-CD44 signaling in the glioma perivascular niche enhances cancer stem cell phenotypes and promotes aggressive tumor growth. *Cell Stem Cell*, *14*(3), 357–369. https://doi.org/10.1016/j.stem.2014.01.005

29. Klank, R. L., Decker Grunke, S. A., Bangasser, B. L., Forster, C. L., Price, M. A., Odde, T. J., SantaCruz, K. S., Rosenfeld, S. S., Canoll, P., Turley, E. A., McCarthy, J. B., Ohlfest, J. R., & Odde, D. J. (2017). Biphasic Dependence of Glioma Survival and Cell Migration on CD44 Expression Level. *Cell Reports*, *19*(3), 668. https://doi.org/10.1016/j.celrep.2017.03.074
30. Kwiatkowska, A., & Symons, M. (2020). Signaling Determinants of Glioma Cell Invasion. In J. Barańska (Ed.), *Glioma Signaling* (pp. 129–149). Springer International Publishing.
31. Chen, X., Wanggou, S., Bodalia, A., Zhu, M., Dong, W., Fan, J. J., Yin, W. C., Min, H.-K., Hu, M., Draghici, D., Dou, W., Li, F., Coutinho, F. J., Whetstone, H., Kushida, M. M., Dirks, P. B., Song, Y., Hui, C.-C., Sun, Y., … Huang, X. (2018). A Feedforward Mechanism Mediated by Mechanosensitive Ion Channel PIEZO1 and Tissue Mechanics Promotes Glioma Aggression. *Neuron*, *100*(4), 799-815.e7. https://doi.org/10.1016/j.neuron.2018.09.046
32. Vassilev, A., Kaneko, K. J., Shu, H., Zhao, Y., & DePamphilis, M. L. (2001). TEAD/TEF transcription factors utilize the activation domain of YAP65, a Src/Yes-associated protein localized in the cytoplasm. *Genes & Development*,

15(10), 1229–1241. https://doi.org/10.1101/gad.888601

33. Baxter, M. E., Miller, H. A., Chen, J., Williams, B. J., & Frieboes, H. B. (2023). Metabolomic differentiation of tumor core versus edge in glioma. *Neurosurgical Focus*, *54*(6), E4. https://doi.org/10.3171/2023.3.FOCUS2379
34. Mohiuddin, E., & Wakimoto, H. (2021). Extracellular matrix in glioblastoma: Opportunities for emerging therapeutic approaches. *American Journal of Cancer Research*, *11*(8), 3742–3754.
35. Aubry, M., de Tayrac, M., Etcheverry, A., Clavreul, A., Saikali, S., Menei, P., & Mosser, J. (2015). 'From the core to beyond the margin': A genomic picture of glioblastoma intratumor heterogeneity. *Oncotarget*, *6*(14), 12094–12109.
36. Miroshnikova, Y. A., Mouw, J. K., Barnes, J. M., Pickup, M. W., Lakins, J. N., Kim, Y., Lobo, K., Persson, A. I., Reis, G. F., McKnight, T. R., Holland, E. C., Phillips, J. J., & Weaver, V. M. (2016a). Tissue mechanics promote IDH1-dependent HIF1α–tenascin C feedback to regulate glioblastoma aggression. *Nature Cell Biology*, *18*(12), Article 12. https://doi.org/10.1038/ncb3429
37. Ananthanarayanan, B., Kim, Y., & Kumar, S. (2011). Elucidating the mechanobiology of malignant brain tumors using a brain matrix-mimetic hyaluronic acid hydrogel platform. *Biomaterials*, *32*(31), 7913–7923. https://doi.org/10.1016/j.biomaterials.2011.07.005

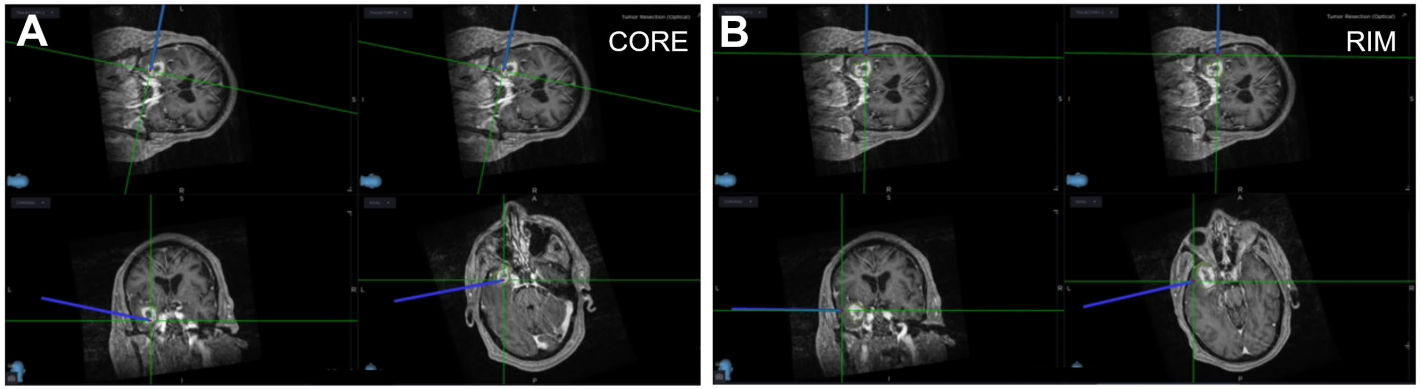

Figure 1. Intraoperative 3D navigation view of GBM core and rim. Tumor biopsies were extracted within the tumor, designated as tumor core (A), and within the invasive margin of the tumor, designated as tumor rim (B).

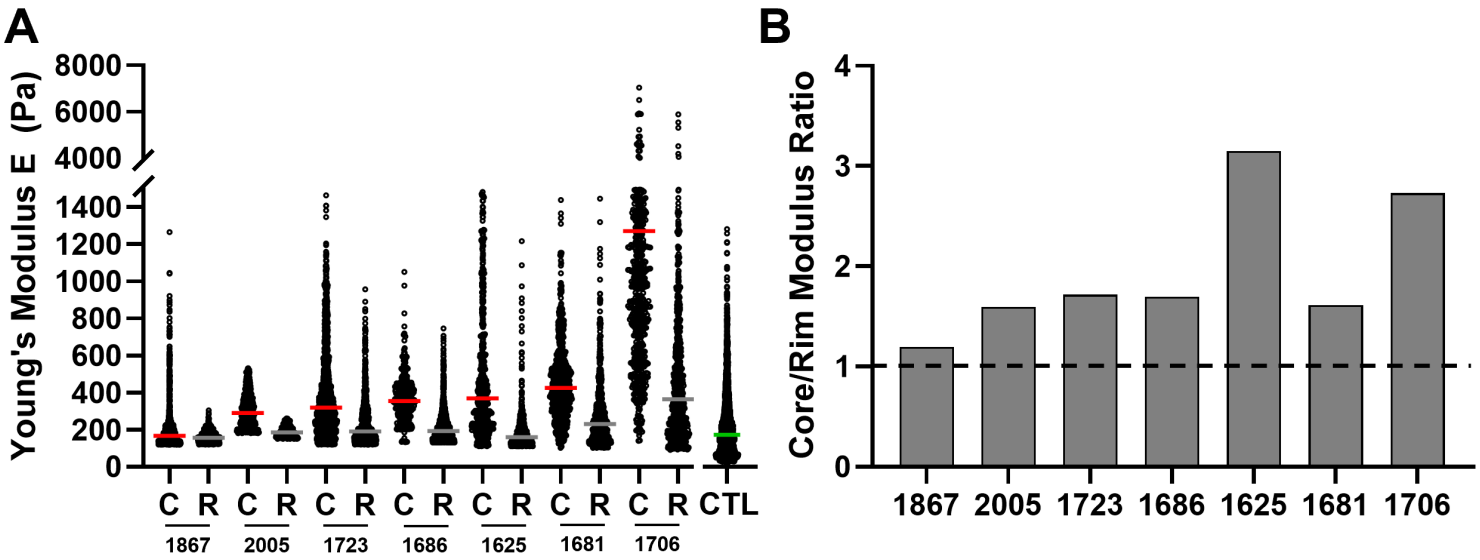

Figure 2. AFM reveals spatial heterogeneity and stiffer core tissue. GBM tumor exhibit heterogeneity in mechanical signatures with tumor core exhibiting higher stiffness when compared to tumor rim and to non-neoplastic controls (A). However, the relative differences between tumor core and rim is patient specific (B).

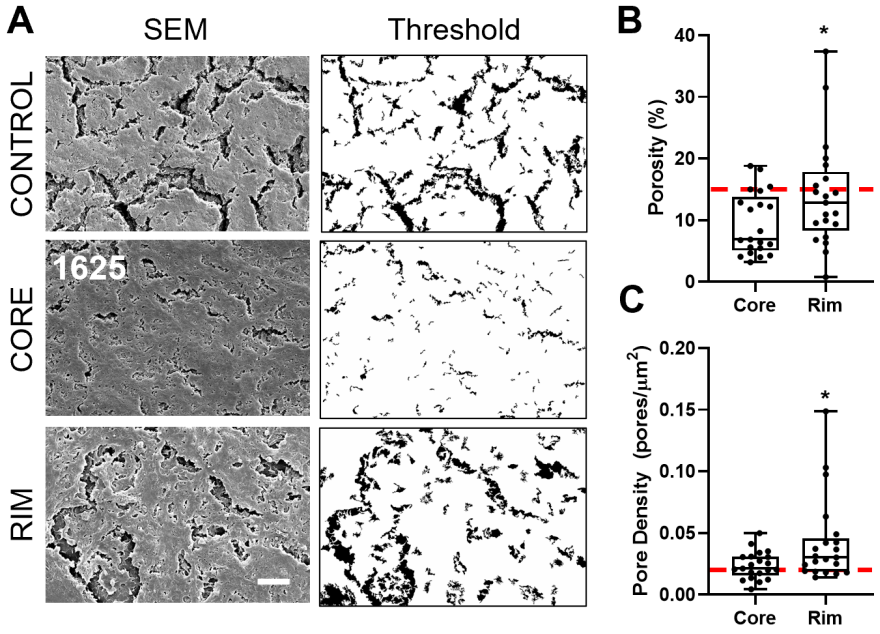

Figure 3. GBM core displays dense ultrastructure with decreased porosity and pore density SEM analysis reveals decreased porosity within tumor cores when compared to tumor rim and control samples (A,B). Pore density, the number of pores per area, was also lower in tumor core (C); * - $p < 0.05$, scalebar = 10 μm

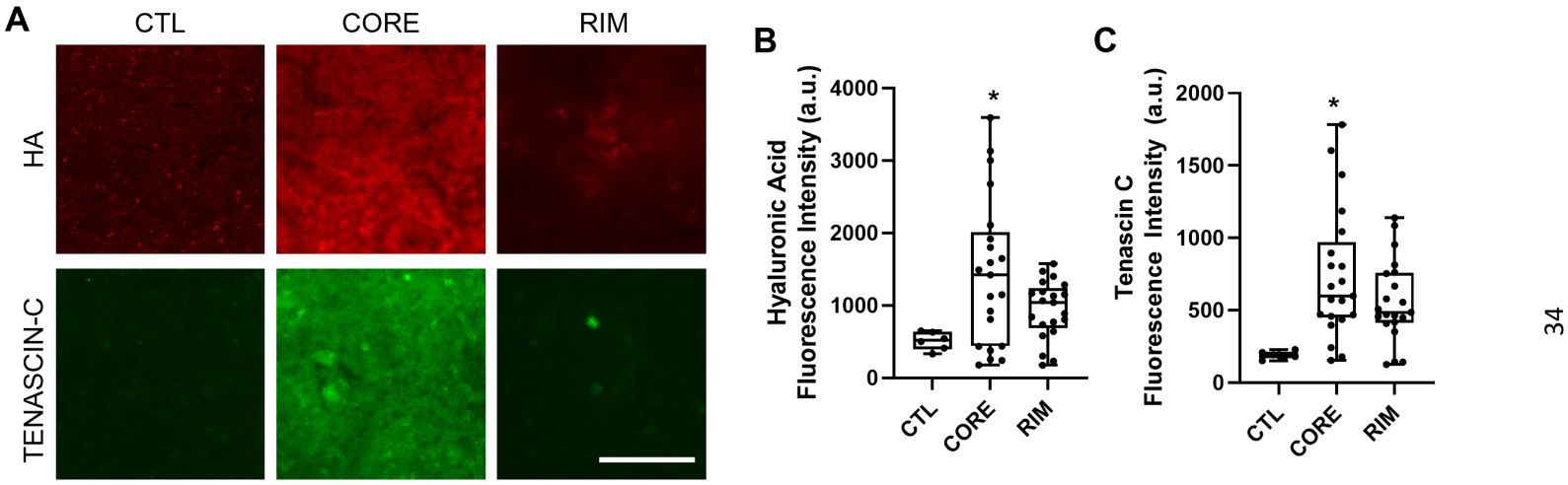

Figure 4. GBM core exhibits high hyaluronic acid and tenascin-C content ECM analysis of tumor core and rim reveal dramatic expression of HA and Tenascin-C in tumor cores while tumor rim exhibits non-significant increases compared to control tissue (A-C). Scalebar = 100 μm

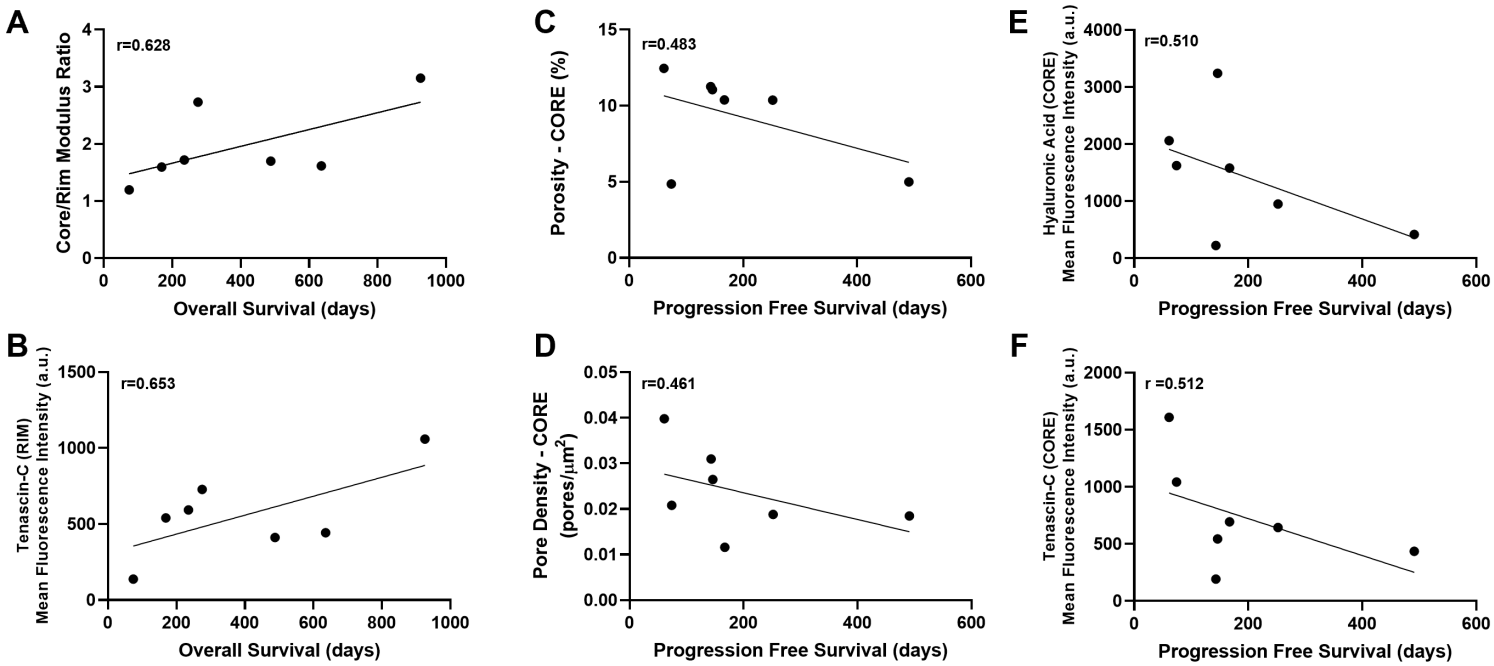

Figure 5. Biophysical signatures of GBM core and rim have prognostic significance Strong positive correlations were noted with core/rim modulus ratio/overall survival and tenascin-C (rim)/overall survival (r >.59) (A,B), while moderate negative correlations were observed with porosity (Core)/progression free survival, pore density (Core)/progression free survival, HA (Core)/progression free survival, Tenascin-C (Core)/progression free survival.

SUPPLEMENTAL FIGURES

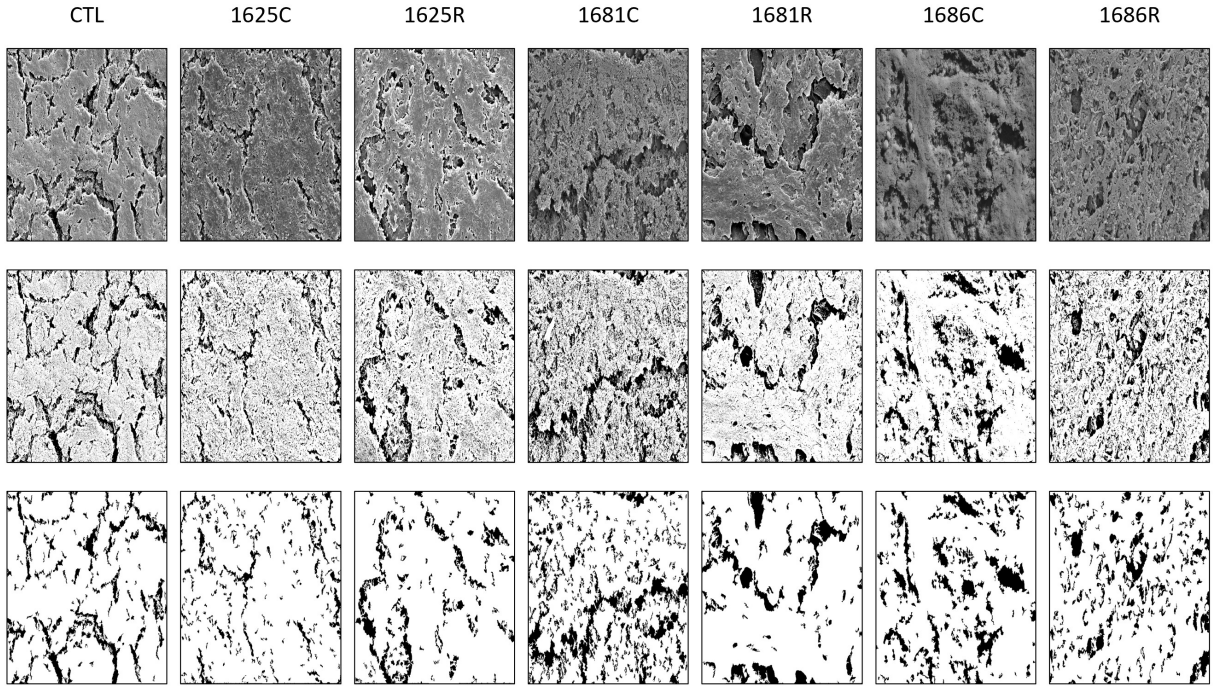

Supplemental Figure 1A: Comprehensive collection of SEM images, raw and under threshold, from our patient cohort, showing their ultrastructural characteristics.

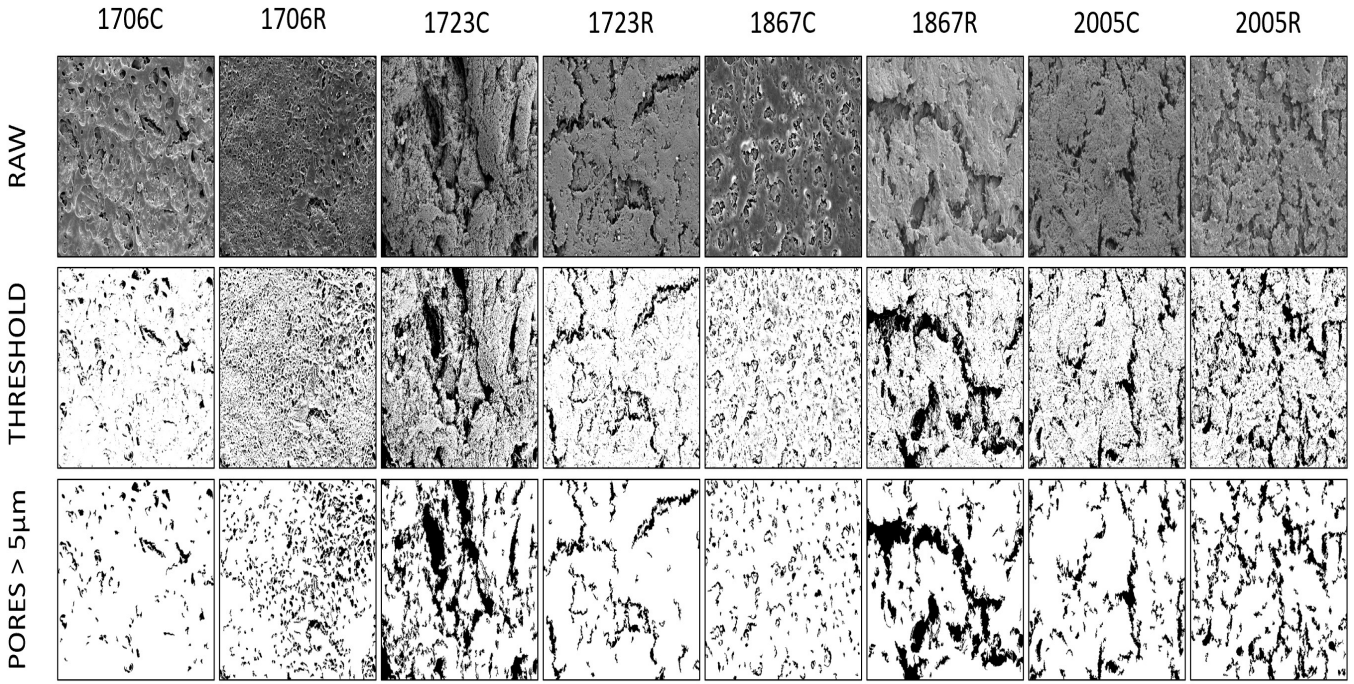

Supplemental Figure 1B: Comprehensive collection of SEM images, raw and underthreshold, from our patient cohort, showing their ultrastructural characteristics.

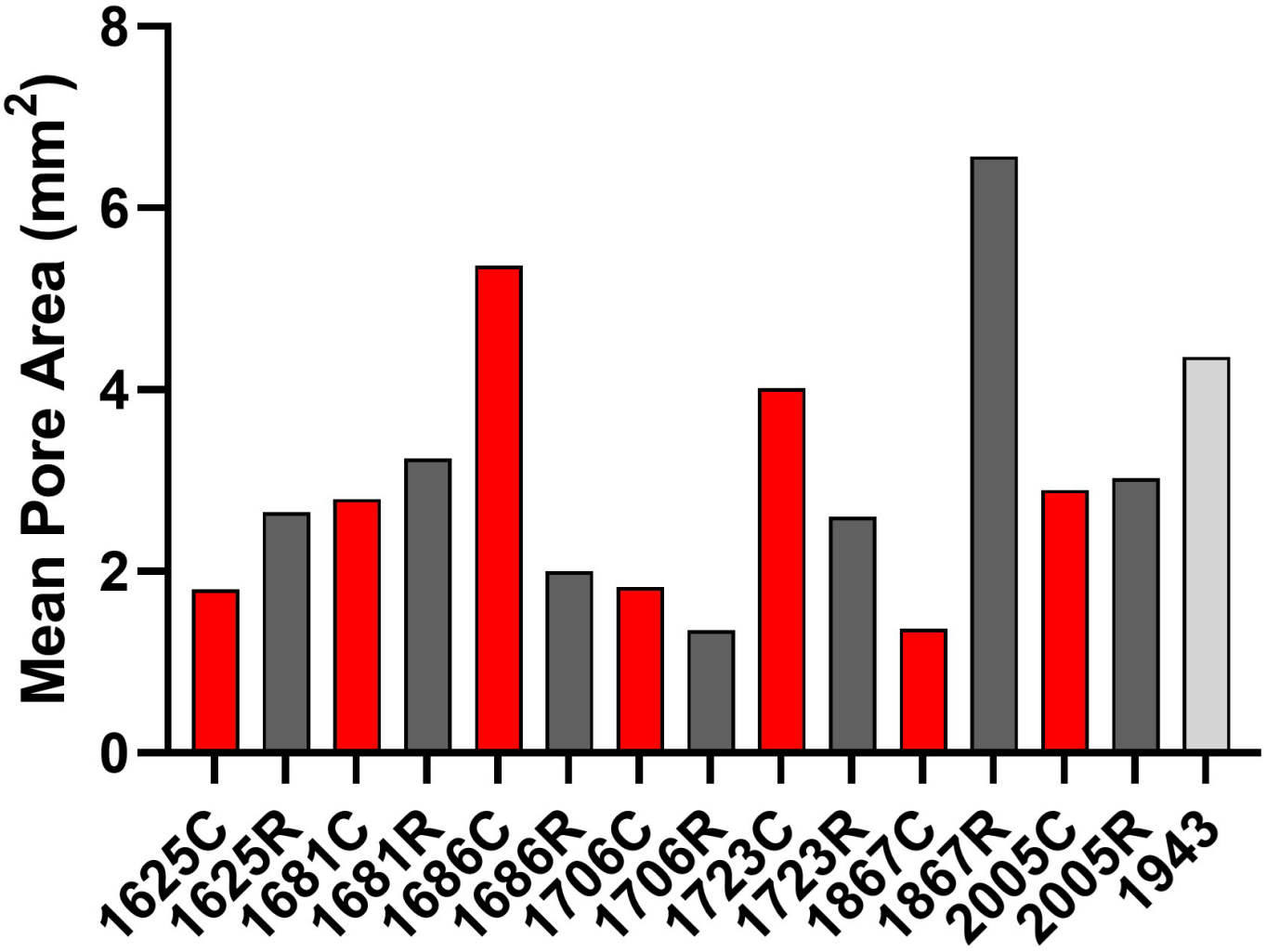

Supplemental Figure 2: Collective results for the mean pore areas of our cohort.

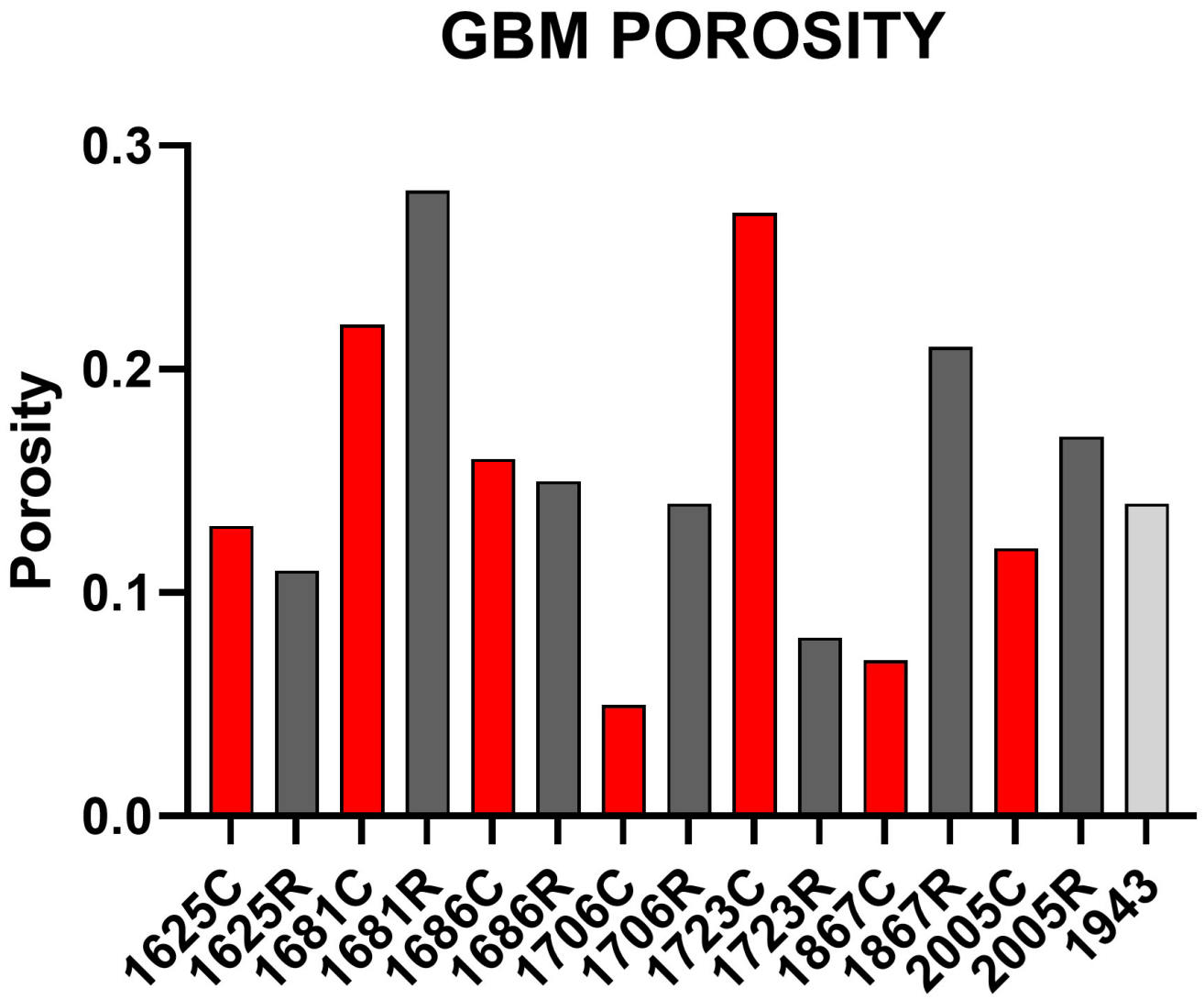

Supplemental Figure 3: Collective results for the porosities of our cohort.

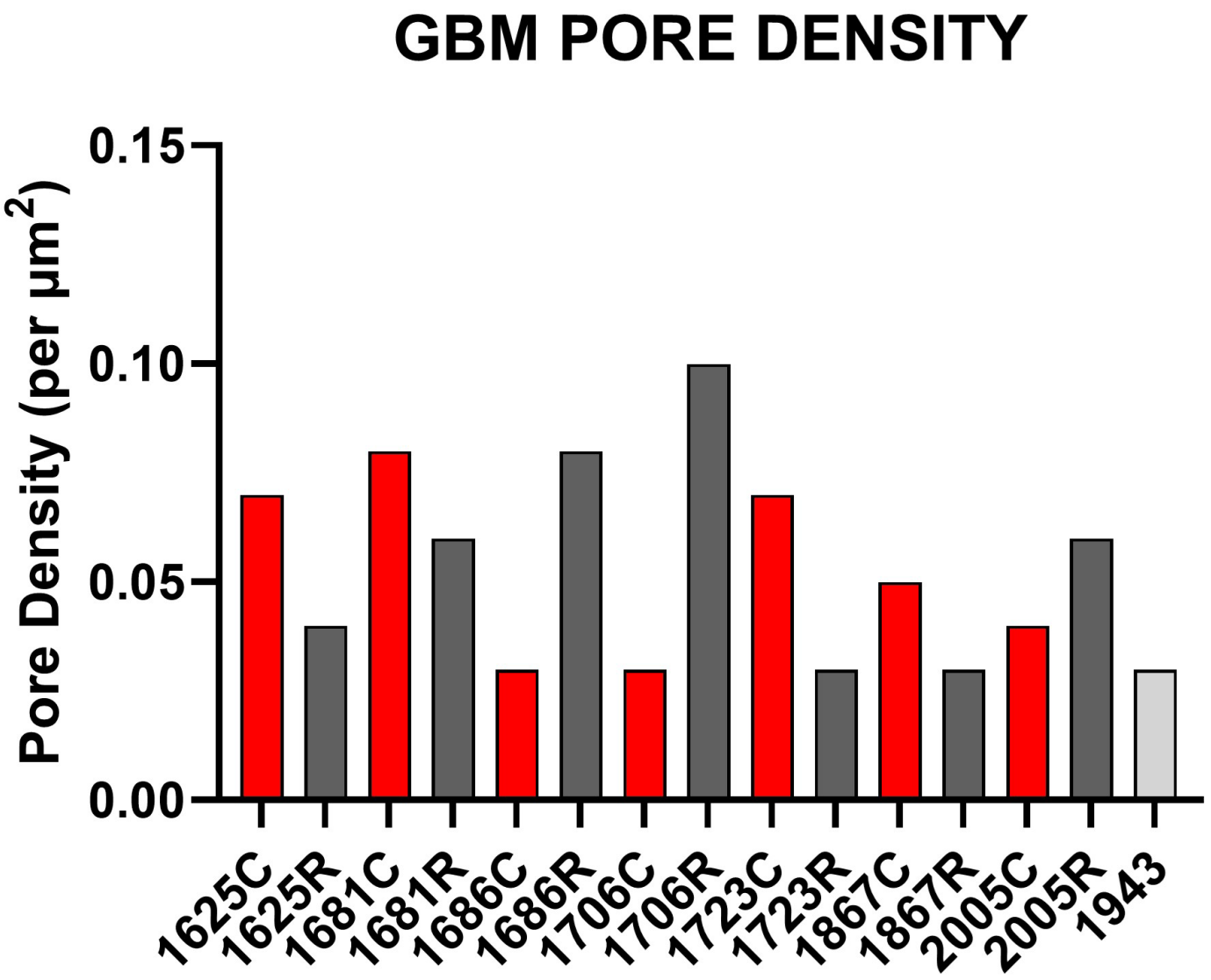

Supplemental Figure 4: Collective results for the pore densities of our cohort.

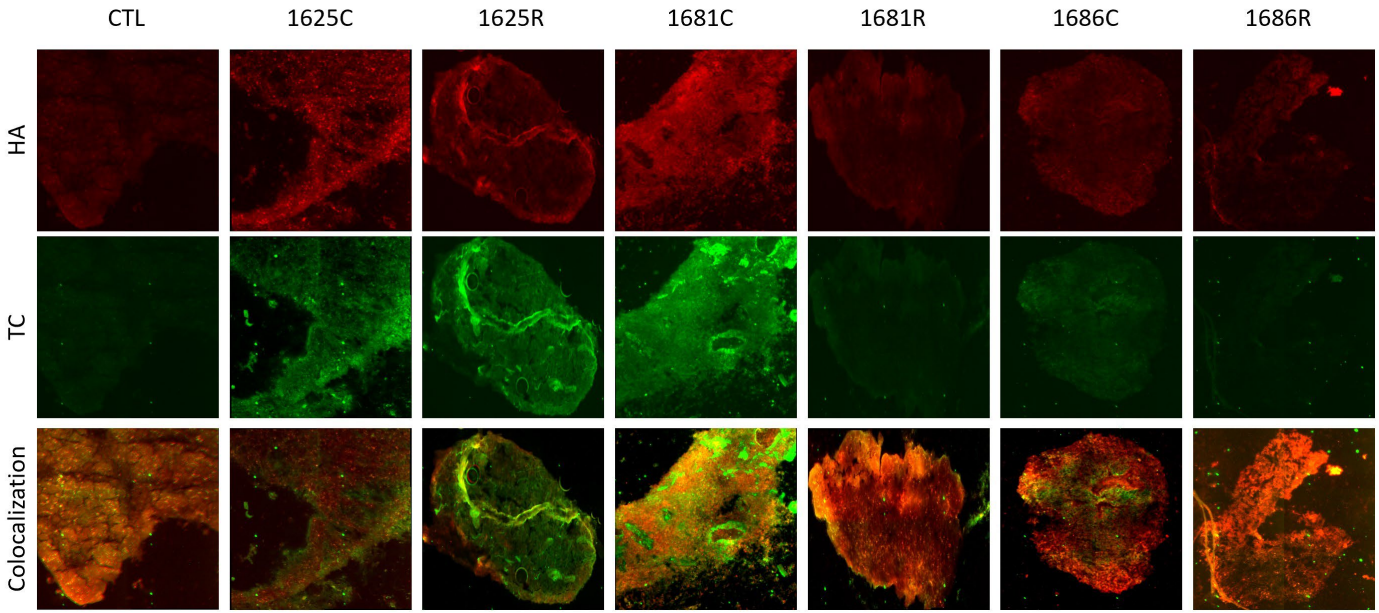

Supplemental Figure 5A: Collective results for the immunofluorescent staining for HA and TC of our cohort.

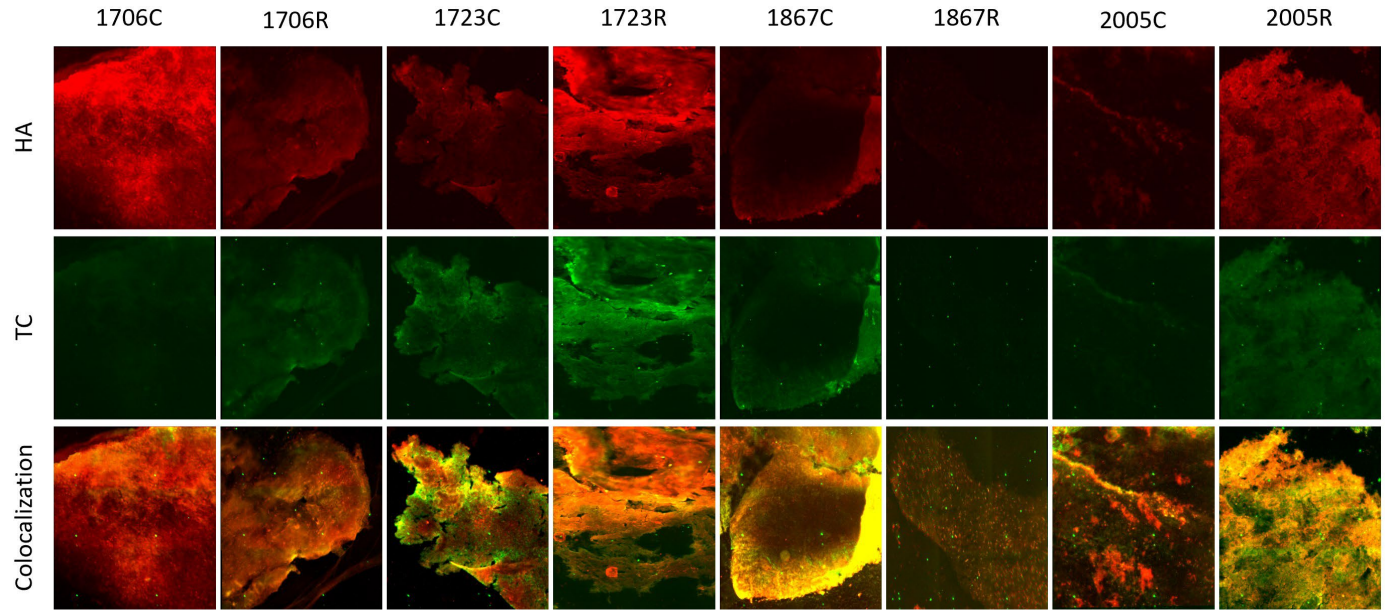

Supplemental Figure 5B: Collective results for the immunofluorescent staining for HA and TC of our cohort.

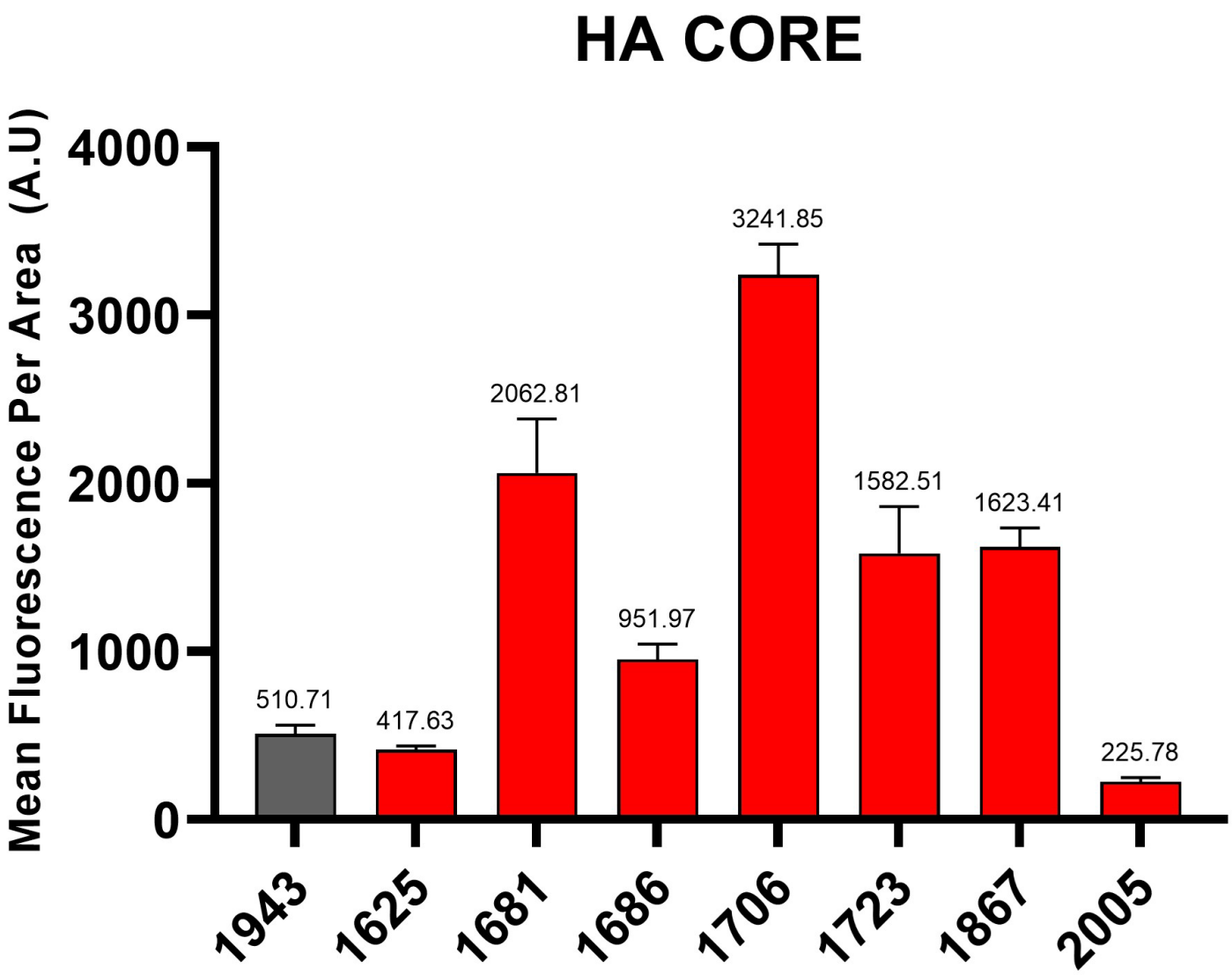

Supplemental Figure 6A: Quantitative results for immunofluorescent staining of HA in core regions.

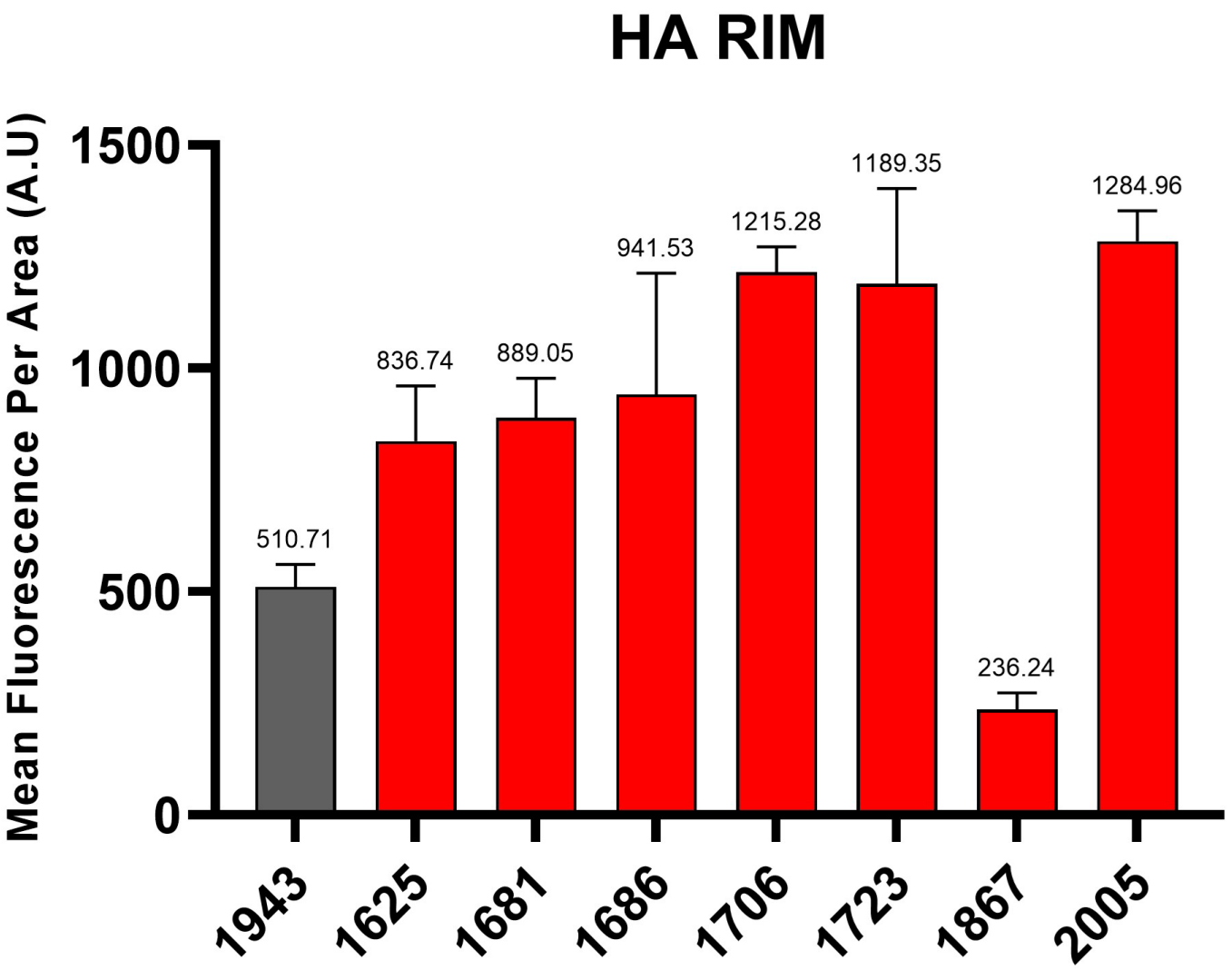

Supplemental Figure 6B: Quantitative results for immunofluorescent staining of HA in rim regions.

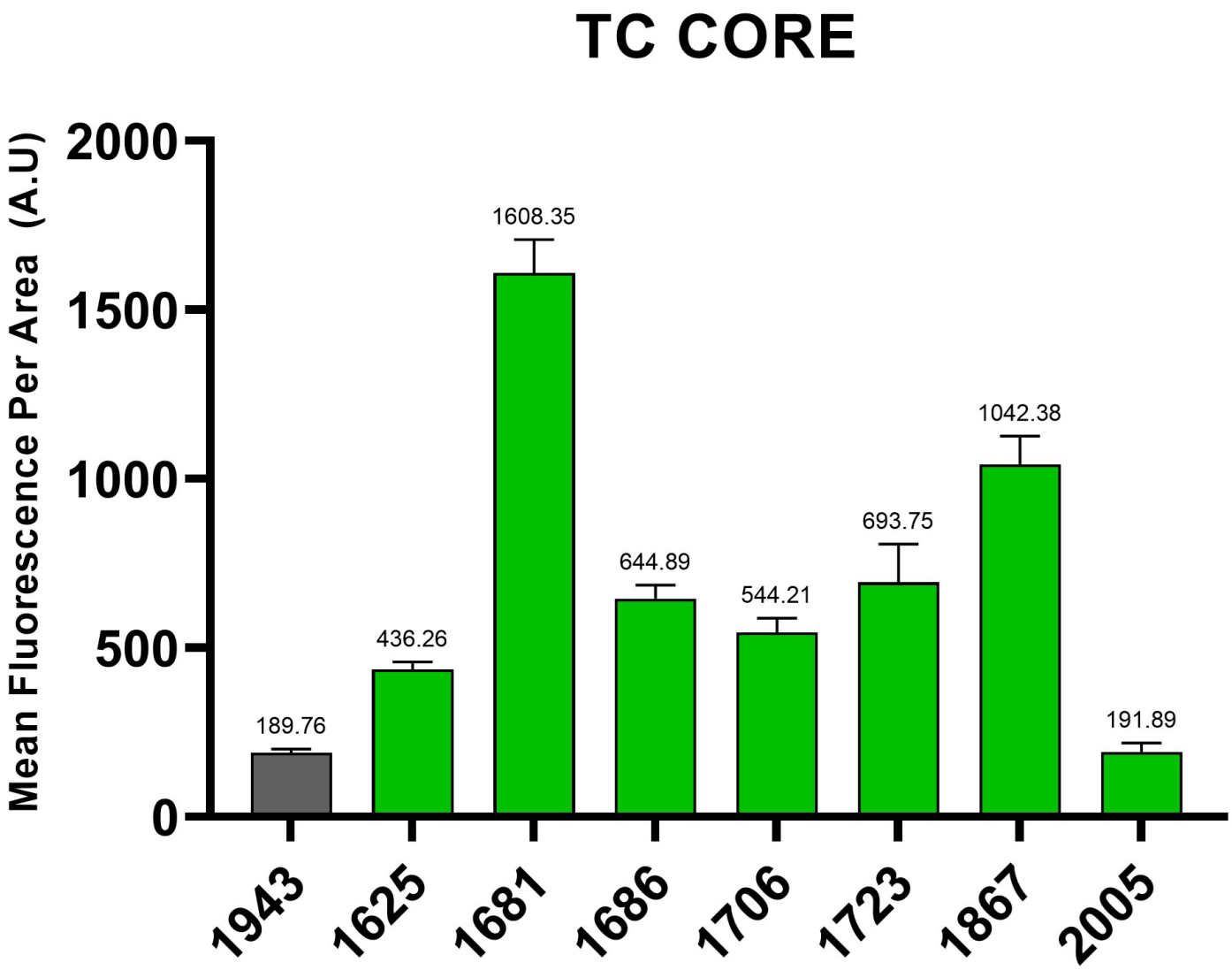

Supplemental Figure 7A: Quantitative results for immunofluorescent staining of TC in core regions.

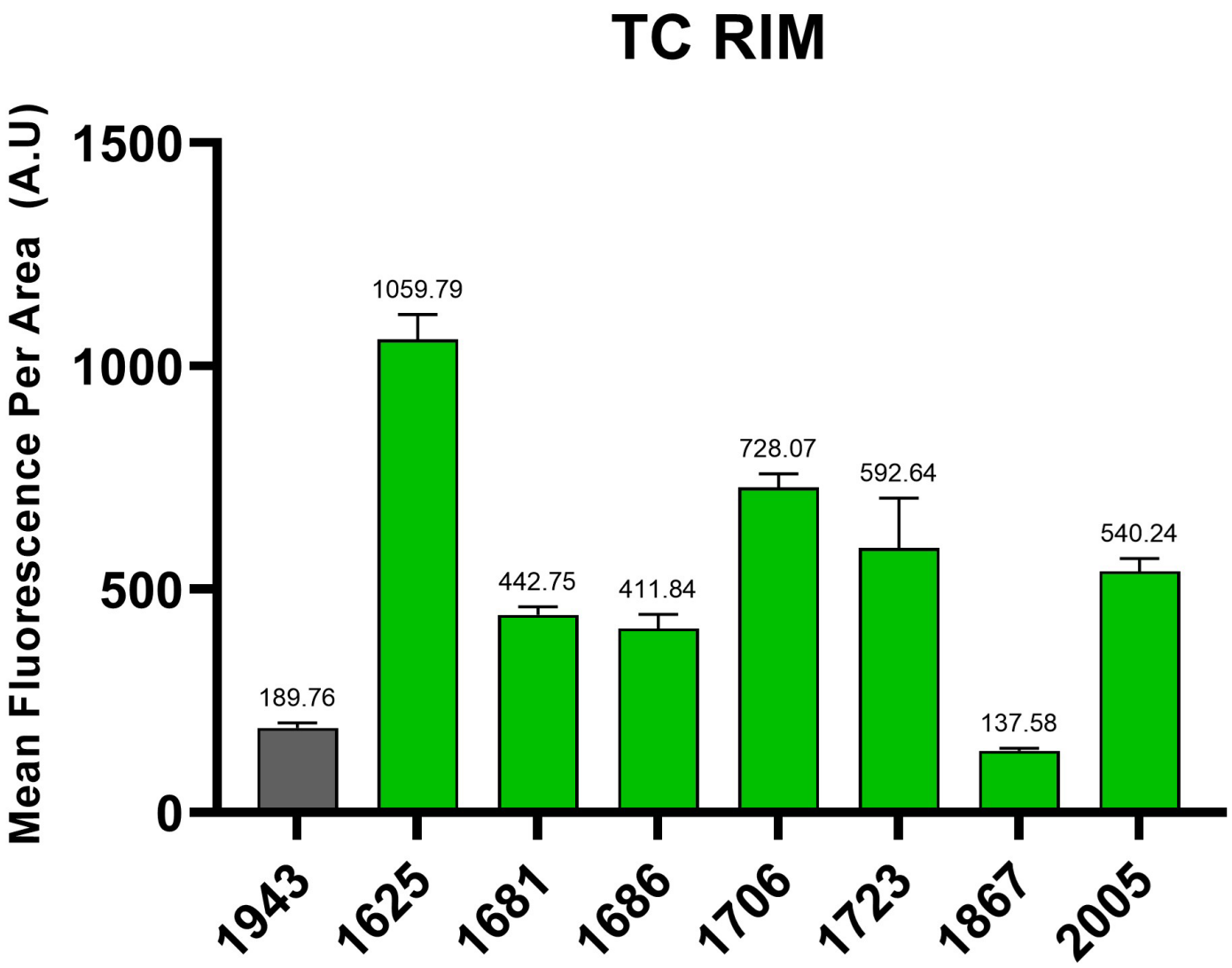

Supplemental Figure 7B: Quantitative results for immunofluorescent staining of TC in rim regions.

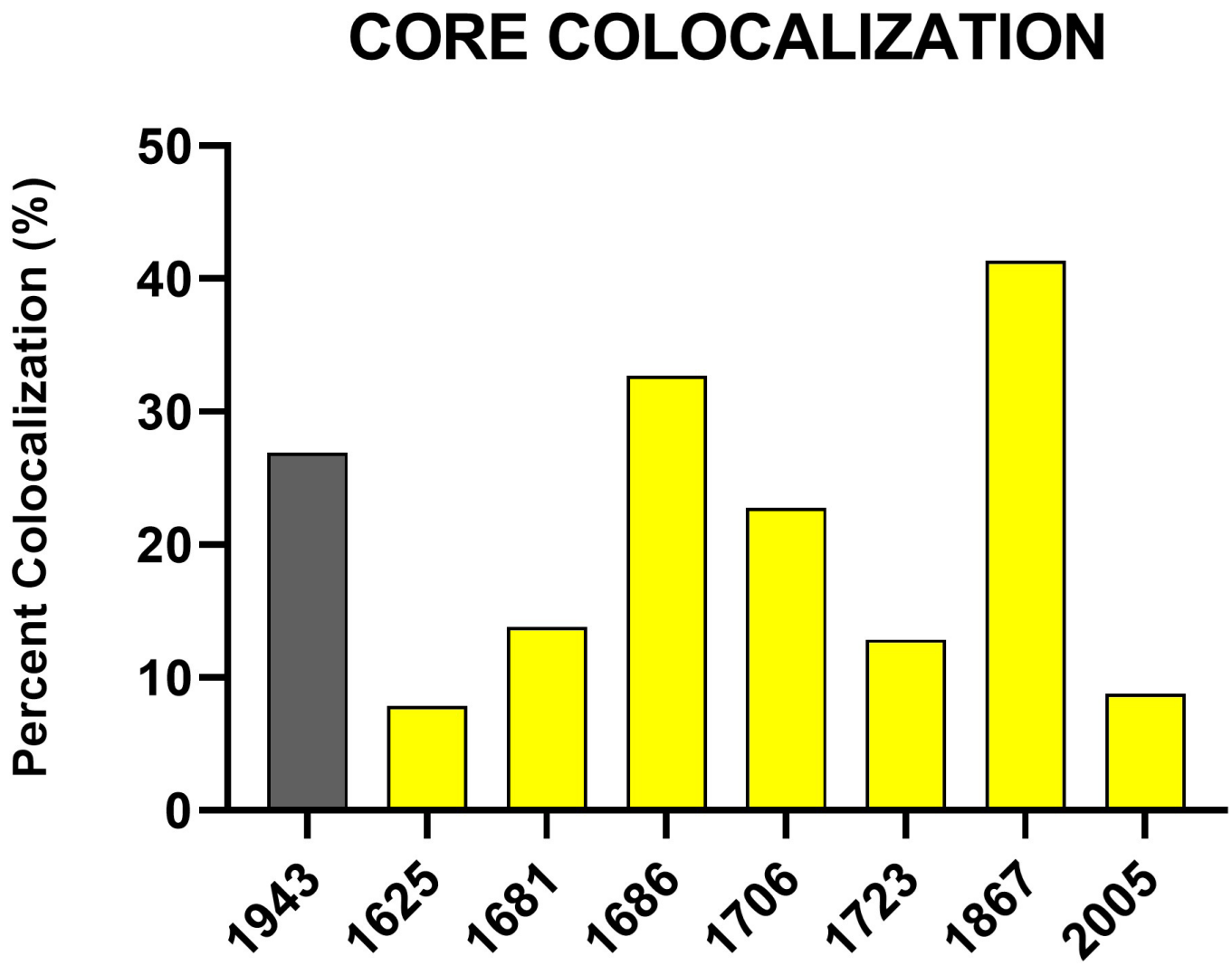

Supplemental Figure 8A: Quantitative results for immunofluorescent HA/ TC colocalization in core regions.

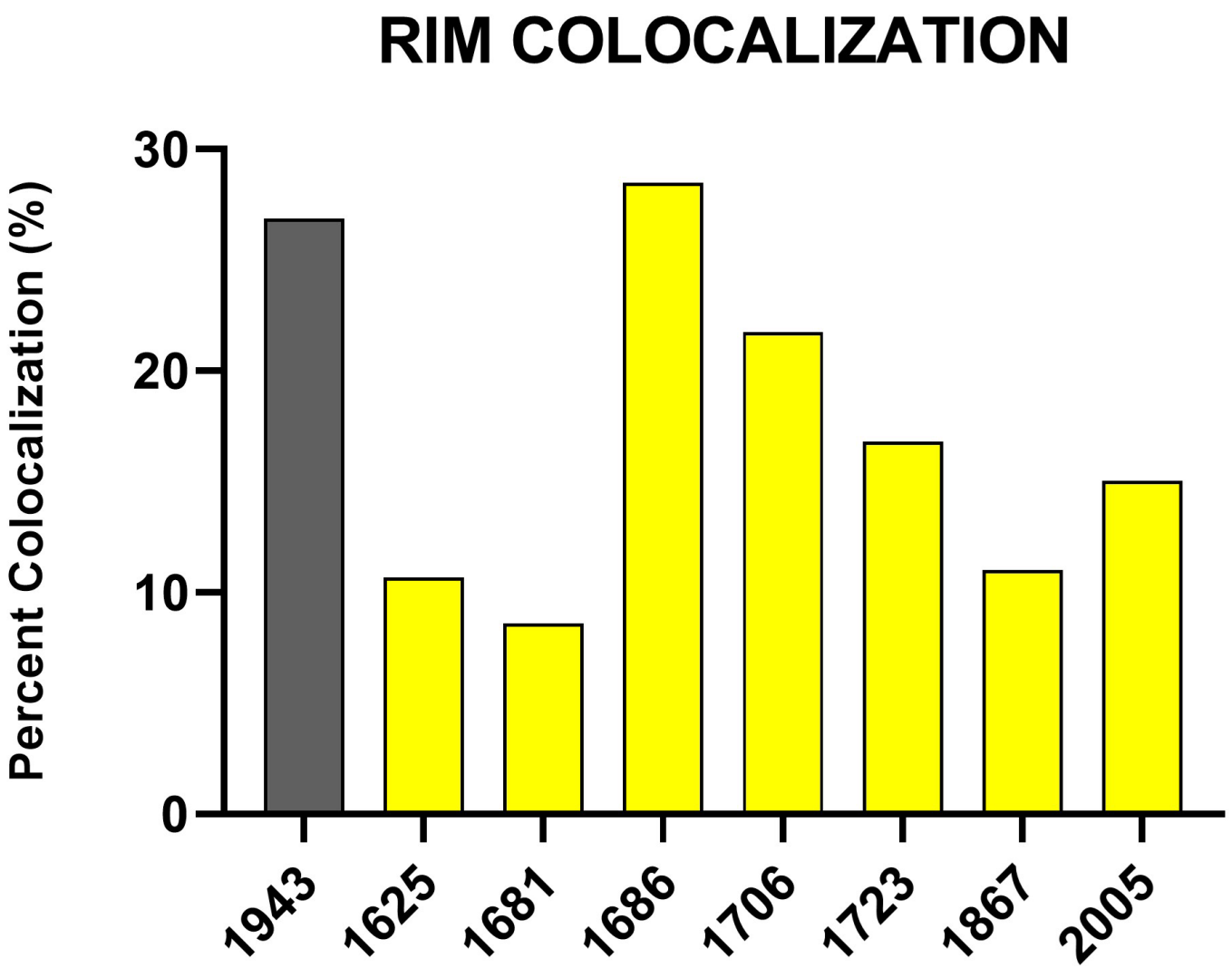

Supplemental Figure 8B: Quantitative results for immunofluorescent HA/ TC colocalization in rim regions.

CURRICULUM VITA

NAME: Bradley James Mahaffey

ADDRESS: 321 Shumaker Research Building
2210 S Brook St
University of Louisville
Louisville, KY 40208

DOB: Louisville, Kentucky – May 30, 1997

EDUCATION &TRAINING: B.S., Physics and Chemistry
Morehead State University
2015-19

PROFESSIONAL SOCIETIES:

Biomedical Engineering Society – BMES – Since 2022

PUBLICATIONS:

Bradley J Mahaffey*, Zachary P Fowler*, Zoe Lung, Vivien Dang, Joseph Chen, “ECM Composition and Organization Underlie Mechanical Signatures of Glioblastoma Core and Rim” Soft Matter (In preparation)

CONFERENCE PROCEEDINGS:

Landon Teer, Dominic Armagno, Bradley Mahaffey, Neha Anil, Marco Munoz, Sihan Sun, Joseph Chen, “Mesenchymal Transitions in Glioblastoma Enhanced Confined Migration Through Nuclear Softening”, Summer Bioengineering Conference, Vail, CO, June 5-9, 2023

Bradley J Mahaffey, Zachary P Fowler, Zoe Lung, Vivien Dang, Neha Anil, Marco Munoz, Joseph Chen, “Quantification of Tumor Biophysical Heterogeneity Through Mechanical and Ultrastructural Analysis”, Summer Bioengineering Conference, Vail, CO, June 5-9, 2023

CONFERENCE PRESENTATIONS:

Bradley J Mahaffey, Zachary P. Fowler, and Joseph Chen, “Biophysical Characterization of Glioblastoma Core and Rim”, KAUST Annual Poster Competition, Thuwal, Saudi Arabia, January 7-13, 2023.

Zachary P. Fowler, Bradley J. Mahaffey, and Joseph Chen, “Glioblastoma Core and Rim Exhibit Distinct Mechanical and Ultrastructural Signatures”, BMES 2022, San Antonio, TX, October 12-15, 2022.